9-10-1997

Type X Silicon Carbide Presolar Grains: Type Ia Supernova Condensates?

Donald D. Clayton
Clemson University, claydonald@gmail.com

David Arnett
University of Arizona

Jave Kane
Lawrence Livermore National Laboratory

Bradley S. Meyer
Clemson University

THE ASTROPHYSICAL JOURNAL, 486:824–834, 1997 September 10

TYPE X SILICON CARBIDE PRESOLAR GRAINS: TYPE Ia SUPERNOVA CONDENSATES?

DONALD D. CLAYTON
Department of Physics and Astronomy, Clemson University, Clemson, SC 29634-1911
DAVID ARNETT
Steward Observatory, University of Arizona, Tucson, AZ 85721
JAVE KANE
Lawrence Livermore National Laboratory, Livermore, CA 94550
AND
BRADLEY S. MEYER
Department of Physics and Astronomy, Clemson University, Clemson, SC 29634-1911
Received 1996 November 20; accepted 1997 April 14

ABSTRACT

In terms of nucleosynthesis issues alone, we demonstrate that the type X silicon carbide particles have chemical and isotopic compositions resembling those from explosive helium burning in ^{14}N-rich matter. These particles are extracted chemically from meteorites and were once interstellar particles. They have already been identified by their discoverers as supernova particles on the basis of their isotopic compositions, but we argue that they are from supernovae of Type Ia that explode with a cap of helium atop their CO structure. The relative abundances of the isotopes of C and Si and trace N, Mg, and Ca match those in the X particles without need of complicated and arbitrary mixing postulates. Furthermore, both C and Si abundances are enhanced and more abundant than O, which suggests that SiC is in fact the natural condensate of such matter. We also briefly address special issues relevant to the growth of dust within Type Ia interiors during their expansions.

Subject headings: dust, extinction — ISM: abundances — ISM: molecules — nuclear reactions, nucleosynthesis, abundances — supernovae: general

1. INTRODUCTION

Silicon carbide particles of type X have been discovered, studied, and characterized isotopically by Amari et al. (1992), Nittler et al. (1995, 1996), and Hoppe et al. (1993, 1994, 1995, 1996a, 1996b); these authors also give references on the history of isolating such particles within the solid residues of meteorites dissolved in acids. The type X particles, called SiC X grains or SiC-X, are characterized and defined by isotopic deficiencies in the heavy isotopes of both C and Si, by their constitutive elements, and by excess ^{15}N (see Hoppe et al. 1994 for definitions of interstellar SiC families). Grains of silicon nitride (Si_3N_4) share the same isotopic peculiarities (Nittler et al. 1995).

These large particles (for interstellar dust: greater than 1 μm) can be analyzed individually by secondary ion mass spectrometry, not only for C and Si isotopes, but also for trace quantities of Ca and Ti isotopes and for excess radiogenic daughters that would identify them as supernova condensates (SUNOCONs). Clear evidence for excess ^{44}Ca, which is attributable to radioactive 47 yr ^{44}Ti decay within those particles, has been demonstrated (Nittler et al. 1996; Hoppe et al. 1996b). This requires the particles to have condensed within supernova ejecta in its first century or so. Because that condensation occurs within the first year after explosion, current uncertainty over the half-life (Kutschera & Paul 1990) is not a significant issue for the X grains, although it is crucial to the question of the ^{44}Ti mass synthesized by the Cas A supernova (The et al. 1995). We will use a 47 yr half-life simply because it is the most common entry in recent data compilations.

Similarly, Amari, Zinner, & Lewis (1996) have demonstrated a clear excess of ^{41}K within low-density grains of graphite (C) owing to radioactive decay (10^5 yr) of ^{41}Ca within the same SUNOCONs. Those authors referred to earlier evidence of excess radiogenic daughter abundances and conclude that the type X particles and many low-density graphite particles are SUNOCONs. Those half-lives are too short for the parent nuclei to have been alive in the solar system, or even to have been abundant in the interstellar medium, which requires that their early condensation be within the expanding supernova gases.

By the same reasoning, excess ^{26}Mg indicates live ^{26}Al within the X particles at extremely high concentrations relative to ^{27}Al, typically ^{26}Al/^{27}Al = 0.1–0.6 (Hoppe et al. 1994 and Table 1; Nittler et al. 1995 and Fig. 4). Those values are much too large to have existed in the solar disk, which also identifies the X particles (and related silicon nitride; Nittler et al. 1995) as presolar grains, probably SUNOCONs. A persistent problem has been that such large ^{26}Al/^{27}Al ratios are found only in the HHe envelopes of stars (Arnett 1996, p. 217), where they exist as remnants of H burning, accompanied by C, N, and Si isotopic ratios that are quite unlike those of X particles. Even there, the mass having a large ^{26}Al/^{27}Al ratio lies in a relatively thin H-burning shell (see Timmes et al. 1995, Fig. 1 near 9 $M_\odot$), and there exists little reason to expect the X-type SiC to have ingested only that aluminum. Table 1 of Meyer, Weaver, & Woosley (1995) shows that the ratio is only about 0.04 in the entire H envelope (or in that envelope plus the HeN shell). Values greater than 0.1 in solid particles are hard to come by, being much smaller in the bulk supernova nucleosynthesis of Al; it would be helpful to have grain condensation directly in the region of production, without the dilution implied by microscopic mixing of other zones. These three radioactive tracers for SUNOCONs were predicted, before their existence was confirmed (Clayton 1975a;

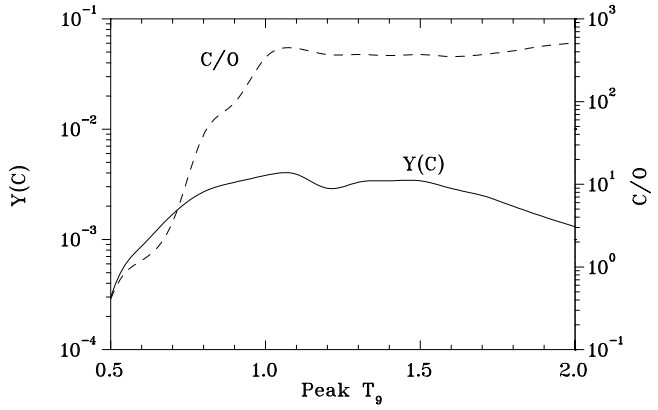

FIG. 1.—Final abundance Y(C) of carbon in each of the 16 separate expansions from the indicated peak initial temperature. The initial density was 10^5 g cm^{-2} in each case. The abundance Y is equal to the number of moles of carbon per gram of total matter. Its final value, near 3×10^{-3} in most zones, is 10-fold greater than the solar abundance, which shows that substantial carbon nucleosynthesis occurs in these zones. The dashed curve shows the abundance ratio C/O, which is much greater than unity. Such values allow carbon dust to grow without danger of oxidation.

Clayton 1977), to be a means of identifing supernova condensates within meteorites. These grains are presolar relics of vast astronomical importance.

In this work, we present evidence that the suite of isotopic signatures carried in these SiC X grains are most easily accounted for, in a nuclear sense, by explosive helium burning at temperatures near or greater than 10^9 K. The natural venue for this would seem to be a cap of He atop a white dwarf that explodes (i.e., a Type Ia supernova).

2. CHARACTERIZING THE SUPERNOVA X PARTICLE AND ITS SOURCE

Because of the large number of related particles now known (Hoppe et al. 1996a, and other papers referred to above), it is useful to target properties of the X particles that may not be shared by all particle types but that seem characteristic of the family. We first offer a short list of isotopes that are common in the X grains but present problems that have defied easy solution. This enables us to identify Type Ia supernovae that are capped with a layer of helium containing unburned ^{14}N as likely sources for the X grains and therefrom to identify a spread of conditions that may relate simply to the observed isotopic spreads of those particles. Constraints from measured properties of these particles are as follows.

1. The production ratio of ^{26}Al/^{27}Al is large, near 0.4. Achieving this ratio in supernovae models is one of the major puzzles and a main purpose of this study.

2. Silicon ratios are near ^{29}Si/^{28}Si $\approx 0.02 \approx$ ^{30}Si/^{28}Si, about half of solar values. Furthermore, the silicon mass fraction should itself be large in order to grow large SiC particles.

3. Carbon production should probably be included in order to achieve C > O and to have enough C to build SiC particles.

4. The carbon is predominantly ^{12}C, which the X particles have in huge excess compared to solar carbon.

5. Local N that can condense (AlN substitutions in SiC or as Si_3N_4) must be ^{15}N-rich. That consistent excess is a defining feature of the X particles and has been a major puzzle.

6. Production of 47 yr ^{44}Ti just prior to the condensation is required. This is a major diagnostic of SUNOCON identity, but it does not require large ^{44}Ti/^{40}Ca production ratios (Nittler et al. 1996) because the particles have chemical fractionation that has enhanced the Ti/Ca element ratio during condensation.

7. Ample ^{41}Ca must be produced near ^{41}Ca/^{40}Ca = 0.01 so that the graphite particles studied by Amari et al. (1996), which carry C, N, and Si isotopes resembling the type X SiC particles, may be linked to them.

Although models of Type II supernovae provide separate regions where one or more of the above may be true, they are not satisfactory sources of X particles because arbitrary microscopic mixing (on the short timescale of explosion) must then be postulated to take one element from one zone, another from another, etc. and then to grow SiC particles (e.g., Nittler et al. 1996). Indeed, multidimensional hydrodynamical calculations (Arnett 1994; Bazan & Arnett 1994; Bazan & Arnett 1997) have shown that one-dimensional simulations of the late stages of such stellar evolution are seriously flawed; qualitatively new phenomena occur even in the two-dimensional case, so that we expect the presupernova models to require significant revision. These new hydrodynamic methods are now being tested directly by experiments on the Nederlandse Ondersoekschool Voor Astronomie (NOVA) laser (Kane et al. 1996); the first results are very encouraging. The simulations in two dimensions correctly represent two-dimensional experiments, and experiments in fully three-dimensional geometry suggest what differences are to be expected. Both theory and experiment suggest that if the simulations do err, they do so toward an excess of mixing. However, simulations of idealized explosions in two dimensions (Arnett 1994; Bazan & Arnett 1997) give macroscopic mixing, but not much of the microscopic mixing needed for the chemical growth of particles that have mixed composition. They certainly do not show the selective mixing needed to make X particles. Although this obstacle may eventually be overcome in a natural way, we are led to rethink the problem.

We recently realized that, from a nuclear point of view, the best way to produce a large ^{26}Al/^{27}Al ratio is by explosive He burning. This was studied long ago by Howard, Arnett, & Clayton (1971), who showed that if a shock can ignite He burning in matter that has not yet burned any He, so that ^{14}N remains as a neutron-poor seed nucleus, the subsequent reactions flow upward near the $Z = N$ line, passing matter through ^{22}Na and ^{26}Al in turn. On the other hand, if any He has burned prior to the arrival of the strong shock, the ^{14}N will already have been converted to ^{22}Ne by successive alpha captures; the matter is now neutron-rich (the neutron excess for ^{22}Ne is $\eta = 0.091$) and the ^{22}Na and ^{26}Al will be bypassed on the neutron-rich side. Howard et al. (1971) abandoned this line of investigation after some study, as have subsequent workers, because in models of Type II supernovae, the shock wave in the He envelope is just not strong enough to provide the burning needed to process matter to ^{26}Al and ^{44}Ti.

However, the helium cap atop a CO white dwarf core that explodes (see Arnett 1996a, pp. 364–371, for references) may afford the venue to reopen this possibility. Its density is high, and the shock will be strong enough to elevate it above $T_9 = 1$ ($T_9 = T/10^9$ K). Our first trial calculation took He plus 1% of ^{14}N by mass at density $\rho = 10^5$ and

TABLE 1

ABUNDANCES IN MOLES PER GRAM AT THE END OF EACH CALCULATION

	PEAK T_9															
^AZ	0.5	0.6	0.7	0.8	0.9	1.0	1.1	1.2	1.3	1.4	1.5	1.6	1.7	1.8	1.9	2.0
^{12}C	3.0E−04	8.7E−04	1.7E−03	2.7E−03	3.3E−03	3.8E−03	3.9E−03	2.9E−03	3.3E−03	3.4E−03	3.4E−03	2.9E−03	2.5E−03	2.0E−03	1.6E−03	1.3E−03
^{13}C	8.6E−13	1.6E−11	1.7E−10	1.8E−10	1.2E−11	3.2E−12	5.8E−13	4.7E−13	4.2E−13	4.1E−13	5.0E−13	9.1E−13	1.5E−12	2.9E−12	5.7E−12	7.9E−12
^{14}C	6.3E−08	2.9E−08	1.6E−14	...	...	...	...	...	...	...	...	...	...	...	...	...
^{13}N	8.3E−12	1.2E−10	9.7E−10	8.2E−10	4.3E−11	9.1E−12	1.4E−12	1.0E−12	8.2E−13	6.7E−13	7.4E−13	1.2E−12	1.7E−12	3.0E−12	5.2E−12	6.5E−12
^{14}N	2.4E−05	1.0E−08	2.2E−13	2.2E−13	2.4E−14	4.7E−16	3.4E−17	5.7E−17	4.3E−17	3.3E−17	2.9E−17	4.6E−17	3.1E−17	3.1E−17	4.1E−17	4.6E−17
^{15}N	1.7E−06	1.3E−06	4.1E−07	8.5E−07	8.2E−10	1.1E−14	8.4E−16	2.5E−15	2.7E−15	2.0E−15	8.0E−16	2.8E−16	3.6E−17	1.3E−17	6.6E−18	3.5E−18
^{15}O	2.6E−06	1.4E−06	3.2E−07	4.9E−07	2.9E−10	1.2E−15	5.6E−17	1.4E−16	1.4E−16	9.4E−17	4.5E−17	1.7E−17	1.6E−18	4.8E−19	1.8E−19	7.2E−20
^{16}O	7.3E−04	7.1E−04	4.9E−04	6.4E−05	3.4E−05	1.1E−05	8.9E−06	7.9E−06	9.1E−06	9.4E−06	9.4E−06	8.4E−06	6.8E−06	4.9E−06	3.4E−06	2.5E−06
^{17}O	1.3E−11	2.0E−12	4.0E−12	2.1E−13	3.7E−15	2.4E−16	4.4E−17	4.9E−17	4.3E−17	3.0E−17	1.6E−17	1.1E−17	1.1E−17	1.7E−17	2.6E−17	2.9E−17
^{18}O	1.6E−06	2.3E−06	2.9E−06	2.8E−06	1.5E−09	6.9E−14	1.2E−14	2.5E−14	3.3E−14	3.5E−14	2.2E−14	8.9E−15	1.5E−15	5.7E−16	3.2E−16	1.9E−16
^{18}F	1.7E−04	1.9E−04	1.9E−04	1.5E−04	6.5E−08	2.5E−12	3.7E−13	6.9E−13	8.5E−13	7.8E−13	4.5E−13	1.6E−13	2.4E−14	8.9E−15	4.5E−15	2.4E−15
^{19}F	3.3E−07	2.1E−06	4.6E−06	1.0E−05	1.8E−08	1.5E−13	1.1E−13	8.0E−13	7.6E−14	4.0E−14	1.0E−14	2.6E−15	3.0E−16	9.3E−17	3.8E−17	1.7E−17
^{19}Ne	1.2E−08	2.5E−08	1.7E−08	1.0E−08	4.7E−12	8.0E−18	3.2E−18	9.3E−18	1.5E−19	1.6E−20	...	...	...	...	...	...
^{20}Ne	8.2E−05	1.0E−04	2.9E−04	4.1E−04	1.7E−04	4.8E−05	4.2E−05	4.4E−05	5.9E−05	6.7E−05	7.0E−05	6.3E−05	4.6E−05	2.6E−05	1.5E−05	9.4E−06
^{21}Ne	1.8E−07	2.6E−07	1.9E−07	1.3E−07	3.9E−09	4.7E−10	4.0E−10	1.9E−09	3.0E−09	3.4E−09	3.4E−09	3.1E−09	2.7E−09	2.2E−09	1.7E−09	1.3E−09
^{22}Ne	6.4E−09	9.6E−08	4.6E−07	6.0E−07	1.1E−07	2.8E−11	3.3E−12	2.2E−11	7.7E−12	2.7E−12	3.1E−13	2.7E−14	8.3E−16	6.7E−17	1.9E−17	9.0E−18
^{22}Na	2.5E−08	5.3E−08	1.3E−06	1.9E−05	4.6E−06	1.5E−09	4.9E−10	2.0E−09	8.8E−10	4.7E−10	1.3E−10	3.3E−11	6.6E−12	2.0E−12	9.4E−13	5.4E−13
^{23}Na	6.3E−06	5.9E−06	5.2E−06	3.4E−06	3.1E−05	3.3E−07	2.3E−09	4.6E−09	1.6E−09	6.8E−10	1.5E−10	5.7E−11	2.7E−11	1.4E−11	7.7E−12	5.0E−12
^{23}Mg	1.7E−13	7.6E−15	1.2E−15	1.1E−15	4.2E−15	5.8E−17	1.0E−19	3.5E−20	...	...	...	...	...	...	...	...
^{24}Mg	2.1E−05	2.3E−05	5.6E−05	3.6E−04	6.7E−04	2.4E−04	2.7E−04	3.7E−04	4.8E−04	5.2E−04	4.4E−04	3.3E−04	1.7E−04	7.6E−05	3.6E−05	2.1E−05
^{25}Mg	1.0E−06	6.6E−07	8.8E−07	9.3E−06	1.2E−04	2.8E−05	1.8E−05	4.2E−05	3.6E−05	2.7E−05	1.4E−05	7.4E−06	2.0E−06	4.4E−07	1.2E−07	4.7E−08
^{26}Mg	4.9E−06	4.9E−06	5.1E−06	6.3E−06	7.5E−06	1.6E−06	9.8E−09	1.9E−08	1.0E−08	5.7E−09	2.0E−09	1.0E−09	4.0E−10	1.9E−10	1.1E−10	7.8E−11
^{26}Alg[a] ...	8.5E−10	1.4E−09	2.3E−09	5.9E−08	2.2E−05	1.4E−05	7.1E−07	1.0E−06	5.7E−07	3.5E−07	1.3E−07	5.8E−08	1.0E−08	1.6E−09	3.5E−10	1.2E−10
^{26}Alm[a] ...	3.1E−14	1.3E−15	3.5E−17	1.5E−18	2.8E−17	1.7E−17	4.7E−19	3.4E−20	...	...	...	...	...	...	...	...
^{27}Al	2.9E−06	2.9E−06	2.8E−06	2.9E−06	1.7E−05	5.1E−05	2.0E−05	3.6E−05	3.2E−05	2.6E−05	1.5E−05	9.5E−06	4.4E−06	2.8E−06	2.1E−06	1.8E−06
^{28}Si	2.3E−05	2.3E−05	2.4E−05	4.2E−05	4.3E−04	1.3E−03	1.4E−03	2.1E−03	1.9E−03	1.5E−03	8.6E−04	5.3E−04	2.3E−04	1.1E−04	6.6E−05	4.5E−05
^{29}Si	1.2E−06	1.2E−06	1.2E−06	1.5E−06	4.5E−06	1.8E−05	9.9E−06	1.3E−05	7.7E−06	5.5E−06	3.6E−06	2.1E−06	9.3E−07	3.7E−07	1.7E−07	9.4E−08
^{30}Si	8.0E−07	8.0E−07	8.1E−07	8.3E−07	1.5E−06	1.3E−05	1.3E−05	1.5E−05	1.0E−05	8.3E−06	6.7E−06	6.2E−06	6.6E−06	7.8E−06	8.2E−06	7.7E−06
^{30}P	1.2E−08	1.1E−08	8.3E−09	7.0E−09	7.3E−08	2.6E−07	3.3E−07	2.7E−07	1.2E−07	8.7E−08	5.1E−08	1.8E−08	4.7E−09	1.6E−09	8.7E−10	5.8E−10
^{31}P	2.6E−07	2.7E−07	2.7E−07	2.7E−07	3.7E−07	2.0E−06	6.8E−06	7.8E−06	9.0E−06	6.2E−06	4.7E−06	4.8E−06	5.1E−06	5.6E−06	5.2E−06	4.4E−06
^{32}P	6.4E−11	1.3E−10	1.7E−10	1.8E−10	3.2E−10	1.6E−09	6.6E−10	8.0E−10	6.3E−10	3.4E−10	1.5E−10	6.0E−11	9.2E−12	1.8E−12	6.2E−13	3.1E−13
^{33}P	9.4E−12	2.4E−11	4.0E−11	5.2E−11	9.5E−11	3.8E−10	6.0E−11	1.0E−10	3.1E−11	1.2E−11	4.4E−12	1.0E−12	1.8E−13	2.9E−13	5.9E−13	8.9E−13
^{32}S	1.2E−05	1.2E−05	1.2E−05	1.2E−05	1.8E−05	1.6E−04	6.9E−04	1.1E−03	9.5E−04	7.5E−04	6.8E−04	5.5E−04	3.9E−04	2.5E−04	1.7E−04	1.2E−04
^{33}S	1.1E−07	1.2E−07	1.2E−07	1.2E−07	1.4E−07	7.3E−07	8.7E−07	1.2E−06	5.3E−07	2.9E−07	1.9E−07	1.1E−07	6.0E−08	6.2E−08	8.2E−08	9.7E−08
^{34}S	5.5E−07	5.5E−07	5.5E−07	5.5E−07	5.3E−07	7.5E−07	2.9E−06	5.0E−06	3.2E−06	2.5E−06	3.4E−06	4.9E−06	8.2E−06	1.5E−05	2.2E−05	2.5E−05
^{35}Cl	7.3E−08	7.4E−08	7.4E−08	7.6E−08	1.0E−07	1.9E−07	9.2E−07	5.2E−06	6.0E−06	7.9E−06	8.9E−06	9.4E−06	1.4E−05	2.2E−05	2.8E−05	2.9E−05
^{36}Cl	1.0E−10	2.0E−10	2.7E−10	2.9E−10	5.7E−10	1.4E−09	1.4E−09	4.3E−09	3.5E−09	3.0E−09	1.9E−09	8.7E−10	2.0E−10	9.4E−11	1.1E−10	1.6E−10
^{37}Cl	2.4E−08	2.4E−08	2.4E−08	2.4E−08	2.3E−08	2.1E−08	1.4E−08	5.0E−09	5.2E−09	4.2E−09	1.6E−09	2.9E−10	2.1E−11	2.1E−11	5.4E−11	1.0E−10
^{36}Ar	2.1E−06	2.1E−06	2.1E−06	2.1E−06	2.2E−06	2.6E−06	1.7E−05	1.6E−04	6.6E−04	1.3E−03	1.8E−03	1.8E−03	1.5E−03	1.0E−03	6.7E−04	4.5E−04
^{37}Ar	2.3E−09	4.6E−09	6.1E−09	6.1E−09	9.9E−09	1.6E−08	3.0E−08	1.5E−07	4.1E−07	5.1E−07	3.6E−07	1.6E−07	4.1E−08	5.3E−08	1.2E−07	1.9E−07
^{38}Ar	4.0E−07	4.0E−07	4.0E−07	4.0E−07	4.0E−07	3.7E−07	3.2E−07	3.9E−07	2.6E−07	2.2E−07	3.6E−07	6.0E−07	1.4E−06	4.5E−06	1.0E−05	1.6E−05
^{39}Ar	1.4E−10	2.9E−10	3.9E−10	4.1E−10	7.0E−10	1.1E−09	1.3E−09	7.4E−10	3.5E−11	1.7E−11	1.7E−11	1.3E−11	5.5E−12	4.8E−12	6.3E−12	7.1E−12
^{39}K	8.9E−08	8.9E−08	8.9E−08	8.9E−08	9.6E−08	1.2E−07	1.8E−07	4.7E−07	1.9E−06	4.3E−06	8.3E−06	1.3E−05	1.9E−05	3.3E−05	4.7E−05	5.5E−05
^{40}K	3.1E−10	4.5E−10	5.5E−10	5.8E−10	8.9E−10	1.5E−09	2.3E−09	3.7E−09	1.5E−09	2.3E−09	2.3E−09	1.4E−09	3.9E−10	2.3E−10	2.4E−10	2.4E−10
^{41}K	6.6E−09	6.6E−09	6.6E−09	6.6E−09	6.5E−09	6.1E−09	4.9E−09	3.8E−09	7.2E−11	1.1E−11	1.6E−11	9.6E−12	1.8E−12	2.6E−12	1.1E−11	3.1E−11
^{40}Ca	1.5E−06	1.5E−06	1.5E−06	1.5E−06	1.5E−06	1.5E−06	1.5E−06	1.9E−06	1.1E−05	9.7E−05	4.4E−04	1.2E−03	1.8E−03	1.7E−03	1.2E−03	8.6E−04
^{41}Ca	1.5E−09	2.9E−09	3.8E−09	4.1E−09	6.9E−09	1.1E−08	2.1E−08	4.0E−08	2.5E−08	3.8E−08	1.0E−07	1.4E−07	9.1E−08	1.1E−07	2.6E−07	7.7E−07
^{42}Ca	1.0E−08	1.0E−08	1.0E−08	1.0E−08	1.0E−08	1.0E−08	1.2E−08	3.3E−08	3.1E−08	1.5E−08	4.9E−08	1.1E−07	1.9E−07	5.7E−07	1.8E−06	4.0E−06
^{43}Ca	2.1E−09	2.1E−09	2.1E−09	2.1E−09	2.1E−09	2.3E−09	2.2E−09	4.8E−09	4.9E−09	2.4E−09	4.9E−09	1.1E−08	1.8E−08	4.5E−08	1.2E−07	2.3E−07
^{44}Ca	3.2E−08	3.2E−08	3.2E−08	3.2E−08	3.2E−08	3.1E−08	2.8E−08	1.9E−08	4.0E−09	9.7E−11	6.7E−10	2.4E−09	3.4E−09	5.5E−09	7.9E−09	8.2E−09
^{46}Ca	6.1E−11	6.1E−11	6.1E−11	6.1E−11	6.2E−11	6.3E−11	7.2E−11	5.4E−10	3.8E−10	7.6E−14	8.2E−17	6.4E−17	1.1E−17	1.0E−17	1.4E−17	1.4E−17

TABLE 1—*Continued*

	Peak T_9															
^{A}Z	0.5	0.6	0.7	0.8	0.9	1.0	1.1	1.2	1.3	1.4	1.5	1.6	1.7	1.8	1.9	2.0
^{48}Ca ...	2.9E−09	2.9E−09	2.9E−09	2.9E−09	2.9E−09	2.8E−09	2.5E−09	1.5E−09	1.0E−10	1.1E−16	...	...	...	...	...	...
^{44}Sc ...	6.8E−14	2.0E−13	4.7E−13	1.0E−12	9.2E−12	3.5E−11	2.2E−10	1.5E−09	2.8E−09	1.6E−09	1.6E−08	7.1E−08	1.1E−07	1.7E−07	2.3E−07	2.2E−07
^{45}Sc ...	8.6E−10	8.5E−10	8.5E−10	8.5E−10	9.7E−10	1.6E−09	3.9E−09	1.1E−08	1.5E−08	4.0E−10	2.5E−09	1.1E−08	2.3E−08	4.7E−08	7.6E−08	8.5E−08
^{44}Ti ...	7.7E−18	7.4E−17	1.8E−15	5.7E−14	1.3E−12	1.8E−11	2.0E−10	3.3E−09	5.9E−08	7.6E−07	1.3E−05	1.3E−04	6.9E−04	1.8E−03	2.8E−03	3.2E−03
^{45}Ti ...	6.9E−19	6.3E−18	3.8E−17	2.6E−16	3.8E−14	7.4E−13	1.1E−11	3.3E−10	4.6E−09	3.9E−09	4.0E−08	2.3E−07	5.6E−07	1.1E−06	1.7E−06	1.8E−06
^{46}Ti ...	4.8E−09	4.8E−09	4.8E−09	4.8E−09	4.8E−09	4.7E−09	4.5E−09	4.6E−09	2.1E−08	8.5E−09	2.4E−08	2.4E−07	8.4E−07	2.0E−06	3.2E−06	3.6E−06
^{47}Ti ...	4.4E−09	4.4E−09	4.4E−09	4.4E−09	4.3E−09	4.2E−09	3.9E−09	2.3E−09	4.0E−09	5.2E−09	5.2E−09	7.9E−08	4.3E−07	1.2E−06	2.3E−06	3.2E−06
^{48}Ti ...	4.5E−08	4.4E−08	4.4E−08	4.4E−08	4.4E−08	4.3E−08	4.1E−08	2.4E−08	8.5E−09	8.3E−10	1.0E−10	3.4E−10	8.9E−10	3.0E−09	9.2E−09	1.8E−08
^{49}Ti ...	3.6E−09	3.7E−09	3.9E−09	3.9E−09	4.3E−09	4.9E−09	6.6E−09	1.7E−08	1.1E−08	3.5E−10	6.7E−13	7.5E−13	1.6E−12	5.5E−12	1.8E−11	3.5E−11
^{50}Ti ...	3.3E−09	3.3E−09	3.3E−09	3.3E−09	3.3E−09	3.4E−09	3.5E−09	7.6E−09	1.2E−08	1.6E−09	3.6E−12	5.3E−16	6.8E−16	2.1E−15	7.0E−15	1.2E−14
^{50}V	1.8E−11	1.8E−11	1.8E−11	1.9E−11	2.2E−11	4.9E−11	1.9E−10	2.1E−09	7.9E−09	2.9E−09	1.8E−11	2.7E−12	7.7E−12	2.7E−11	8.9E−11	1.7E−10
^{51}V	7.4E−09	7.3E−09	7.3E−09	7.3E−09	7.2E−09	7.1E−09	6.7E−09	5.8E−09	1.1E−08	8.0E−09	8.3E−11	2.1E−12	8.2E−12	5.2E−11	2.2E−10	5.5E−10
^{48}Cr ...	5.1E−20	5.9E−19	4.0E−18	2.3E−17	2.9E−15	7.2E−14	1.5E−12	2.3E−11	1.2E−09	4.6E−08	1.0E−07	1.0E−06	1.1E−05	5.7E−05	1.8E−04	4.3E−04
^{49}Cr ...	1.6E−20	2.1E−19	1.7E−18	9.9E−18	5.7E−16	5.4E−15	6.6E−13	8.4E−12	1.5E−10	3.9E−09	3.2E−09	1.9E−08	1.5E−07	7.2E−07	2.4E−06	5.3E−06
^{50}Cr ...	1.5E−08	1.5E−08	1.5E−08	1.5E−08	1.4E−08	1.4E−08	1.3E−08	5.2E−09	2.7E−09	1.1E−08	1.3E−08	2.9E−08	3.2E−07	1.8E−06	6.5E−06	1.5E−05

[a] ^{26}Alg is the ground state of ^{26}Al, while ^{26}Alm is the first excited (metastable) state of ^{26}Al.

shocked it up to $T_9 = 1$. This first calculation gave the following isotopic results and flow information.

2.1. *Clues from an Expansion from* $T_9 = 1$

1. The $^{26}Al/^{27}Al$ production ratio was 0.4, just as needed. In addition, X(Al) = 10^{-3}, which was much larger than solar, showing that there was net production of elemental Al from seed ^{14}N.

2. Silicon ratios were near $^{29}Si/^{28}Si \approx 0.02 \approx {}^{30}Si/^{28}Si$, much less than solar. Furthermore, $X(Si) = 0.01$, which was much larger than solar and showed net production of ^{28}Si from the new ^{12}C that has been fused by the triple alpha reaction.

3. Carbon production was surprisingly large, having a surviving mass fraction $X(C) = 0.05$, which is about 80% of all the ^{12}C newly fused by the triple alpha reaction. This puzzled us until we studied the timescales. Total production of ^{12}C (near 6%) is impulsively concentrated toward $t = 0$. But the reaction rate $\langle N_A \sigma v \rangle$ is small for $^{12}C(\alpha, \gamma)$, so that only about one-fifth of that ^{12}C can process onward during time available. As $\langle N_A \sigma v \rangle$ is bigger for ^{16}O, ^{24}Mg, and ^{20}Ne, this matter passes upward to ^{28}Si, where the flow stalls. Thus we have C > O in the final abundances, and the carbon dust will not be oxidized. This is needed to make SiC. The largest two abundances are $X(C) = 5\%$ and $X(Si) = 1\%$. So, the only condensate other than carbon itself that can condense abundantly is SiC! The composition of this trial expansion has even identified SiC as the main condensate; only graphite could be more abundant. This is a common feature of explosive helium burning; see also the "low" density (10^6 g cc^{-1}) case in Arnett (1997).

4. The carbon was pure ^{12}C.

5. The nitrogen was virtually pure ^{15}N at $T_9 = 1$ instead of the solar value $^{14}N/^{15}N = 272$. Interestingly, this ^{15}N is synthesized primarily as ^{15}O, which decays after freezeout. Original N, which is ^{14}N, remains abundant only in matter that is heated to less than $T_9 = 1$. This suggests an interesting dependence on timescales and temperatures. The mass fraction $X(N)$ is not too small, offering encouragement for AlN or Si_3N_4 inclusion or separate condensation.

6. The ^{44}Ti mass fraction was small, but will be much larger in portions of the He cap heated to a greater peak temperature.

3. SURVEY OF BURNING RESULTS

Considerably encouraged by the exploratory $T_9 = 1$ calculation above, we have surveyed the explosive burning of helium in the relevant range of temperatures. In this survey, we use a complete nuclear network written by one of us (B. S. M.; see Meyer, Krishnan, & Clayton 1996). It extends to lower density an independent survey that two of us (J. K. and D. A.) have conducted for the exploration of nucleosynthesis from the vigorous detonation of helium. We take as initial values the full set of abundances after processing the solar abundances by hydrogen burning at constant $T = 50$ MK until H exhaustion. We then assume that composition to be shock heated to a maximum temperature of $T_{9\,\max}$, following which the temperature and density decline with the usual parameterized timescale in seconds $\tau = 446\ \rho^{-1/2}$. This conventional parameterization leaves the initial temperature and density as the two parameters of the survey. In what follows, we present results from this survey using an initial density of $\rho = 10^5$ g cm^{-3}, unless specified otherwise. The survey is then over the single parameter $T_{9\,\max}$. We chose 16 discrete values for $T_{9\,\max}$ ranging between 0.5 and 2.0. The final abundances are taken to be those at the point when the temperature has fallen to $T_9 = 0.08$ because negligible changes can occur beyond that point in time (i.e., at lower temperature) apart from decay of radioactive species.

Figure 1 displays the carbon abundance $Y(C)$ and its ratio to the oxygen abundance (scaled on the right ordinate). As $T_{9\,\max}$ increases from 0.5 to 1.0, the triple alpha reaction is able to synthesize increasingly more carbon before the density declines to a value too small for its rate (per cm^3), which is proportional to $Y(C)^3$. Between $1.0 < T_{9\,\max} < 1.5$, the rate of the $^{12}C(\alpha, \gamma)^{16}O$ reaction becomes more effective at siphoning off the ^{12}C and moving much of it to ^{16}O and beyond. However, the C/O ratio is always very large because the synthesized nuclei tend to either remain at ^{12}C or to be processed past ^{16}O. That is, ^{16}O is not a favored final destination for the flow. This is of significance for the condensation of SiC. The large C/O ratio throughout all zones ensures that oxidation of carbon dust is not a worry; there is insufficient oxygen to oxidize all but a small amount of the carbon.

This carbon is almost isotopically pure ^{12}C; typically, $^{12}C/^{13}C = 10^6$ for individual zones. The ^{13}C that is produced is dominated by the radioactive ^{13}N content at freezeout. This is encouraging but too much of a good thing. The observed X grains have $^{12}C/^{13}C$ ratios lying between 165 and 2500 (Hoppe et al. 1994). Although these are sufficiently ^{12}C-rich to identify these particles as SUNOCONs, it raises the question of what the source of the few ^{13}C atoms in these particles is. In the scenario we propose here, the most likely ideas may be related to the collisions of these fast SUNOCONs with preexisting carbon dust from a circumsupernova region or to the ^{13}C-rich carbon at the surface of the He cap within the ^{14}N-dominated matter. The latter may also be required as a source for the ^{14}N within the X grains. Be that as it may, we count the C abundance, the C/O ratio, and the $^{12}C/^{13}C$ ratio as strong positive correlations between the observed particles and these calculated abundances.

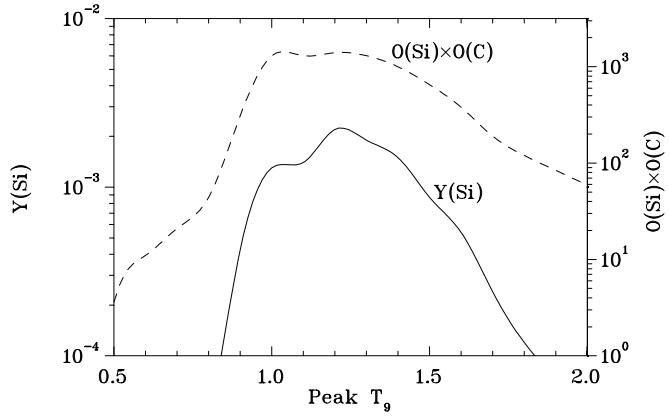

FIG. 2.—Final abundance $Y(Si)$ of silicon in each zone exceeds the solar value 2.3×10^{-5} in each of the zones and by a factor of ~ 100 at the peak of Si production. This large abundance enhances the condensation of SiC grains during the expansion of the zone, leading to our thesis that the X type SiC grains may be SUNOCONs. The dashed curve shows that the product of the overproductions of Si and of C with respect to solar abundances are near 1000 at the maximum. This suggests SiC growth in this matter.

Figure 2 shows both the final abundance of silicon and its product with the carbon abundance. The broad Si abundance peak is greater than $Y(\mathrm{Si}) = 10^{-3}$ Si nucleon^{-1} for $T_{9\,\mathrm{max}}$ between 1.0 and 1.5. Note first that this large amount of silicon demonstrates production of Si, whose solar abundance is 2.3×10^{-5} Si nucleon^{-1}. Even averaged over all 16 zones, the Si overabundance is 32 times its initial (solar) value. Within its abundance peak between $1 \leq T_9 \leq 1.5$, the abundance $Y(\mathrm{Si})$ is almost equal to that of C and is greater than that of any other element, save He. This therefore appears to be an ideal nuclear process for making material that will condense SiC. The basic reason is both simple and satisfying: after production of ^{12}C, the alpha captures tend to move the nuclei rapidly through ^{16}O, keeping its own abundance small, but stalling at ^{28}Si (below $T_{9\,\mathrm{max}} = 1.5$), where the capture rate is too small to move on up the line. Because of this, ^{28}Si is typically the second most abundant nucleus synthesized for $T_9 < 2$.

Other factors being equal, enhanced abundances for both C and Si clearly encourage the growth of larger SiC particles. The observed SiC particles have been puzzlingly large for SUNOCONs, so perhaps these enhanced abundances will be helpful in that regard. From purely kinetic factors, the rate of growth of SiC mass will be proportional to the density n(C) times the density n(Si). A relatively dramatic example lies in the range $T_9 = 1$ to 1.5 , where the final overabundances with respect to solar abundances nucleon^{-1} are, respectively, $\mathcal{O}(\mathrm{C}) = 3 \times 10^{-3}/2.5 \times 10^{-4} = 12$ and $\mathcal{O}(\mathrm{Si}) = 2 \times 10^{-3}/2.3 \times 10^{-5} = 87$. The enhancement of the kinetic collisions rate over that with solar abundances is therefore $12 \times 87 \approx 1000$. Figure 2 contains the product of these two overabundance factors as a function of peak temperature. Since the surface area of the SiC particle is larger for larger particles, the rate of growth of the particle radius is linear in time if the number densities are constant (Clayton & Wickramasinghe 1976, eq. [10]). If the size of SiC (assumed, for sake of discussion, to be grown from C nucleations) is taken to be proportional to the flux of Si atoms, then this composition would grow SiC particles 87 times larger than would solar composition on the same adiabat. Stated more generally, this large overabundance product for $\mathcal{O}(\mathrm{C}) * \mathcal{O}(\mathrm{Si})$ may help overcome the disadvantage of the rapid expansion of Type Ia He caps.

This silicon is ^{28}Si-rich. When averaged over all 16 zones, the ^{29}Si and ^{30}Si abundances remain near solar, whereas the ^{28}Si overabundance is a factor of 32 times solar. Figure 3 displays the ^{29}Si and ^{30}Si excesses in the delta notation (parts per thousand excess of that isotope relative to ^{28}Si when compared with the solar ratio). They show clearly that between $T_9 = 1$ and 1.5, where the Si production is greatest, the ^{29}Si and ^{30}Si deficiencies are greatest. This certainly supports the supposition that the observed particles, having deltas near -500 for both heavy isotopes (i.e., isotopic ratios near half solar), may have condensed from this matter.

Having found the C, O, and Si abundances and isotopic ratios to be ideal for SiC condensation, we look at some of the more important trace elements measured within SiC particles. These are elements that are not stoichiometrically part of the SiC structure but that are accommodated to varying degrees within it. Probably the most important are Mg, Ti, and N because their extreme isotopic values are universally recognized as important clues to the correct genesis of these particles. Figure 4 shows the largest production ratios ever calculated for ^{26}Al/^{27}Al within stellar ejecta. Values as large as 1 occur near $T_{9\,\mathrm{max}} = 0.8$. This peak is fairly narrow in comparison to the yield of Si (Fig. 2). The elemental overabundance of aluminum, $\mathcal{O}$(Al), is also shown on the right ordinate of Figure 4. It confirms that Al is also overabundant in the lower range of temperatures. Even in the 16 zone superposition, Al is overabundant by a factor of 4, which is mostly from $T_9 < 1.5$. We stress the high ^{26}Al/^{27}Al ratios within enhanced Al abundances, a result that is novel in Al production studies.

The sharpness of the peak in ^{26}Al/^{27}Al ratio results from its requirement of seed ^{14}N for the production of ^{26}Al (which is also true for ^{22}Na). If $T_{9\,\mathrm{max}}$ is too large, the original ^{14}N seeds are processed up the line past A = 26. Howard et al. (1971) had already shown large ^{22}Na production near $T_{9\,\mathrm{max}} = 0.6$ for the same reason. Some of the elemental Al production occurs at higher T (see right ordinate in Fig. 4), because it is, like ^{28}Si, grown in part from the ^{12}C that is made by the triple alpha reaction. But the chain

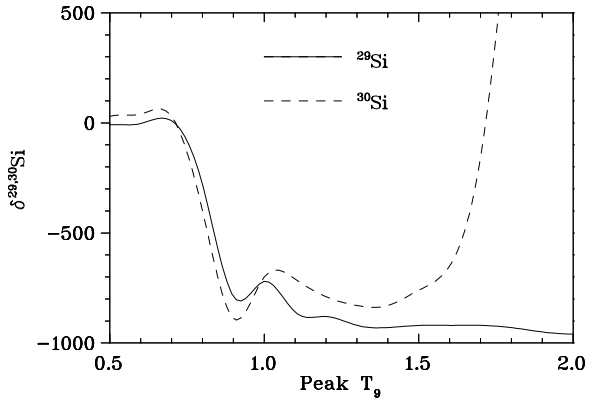

FIG. 3.—Isotopic composition of the final silicon is shown in delta notation, which is the deviation from solar isotopic ratios in parts per thousand. The isotopic compositions are near solar near the surface but plunge to large deficiencies of both ^{29}Si and ^{30}Si at initial temperatures greater than 0.7 GK. This large deficit, which is by nearly equal amounts for both heavy isotopes, occurs where the Si production peak occurs (Fig. 2). These isotopic characteristics are also those of the SiC X grains.

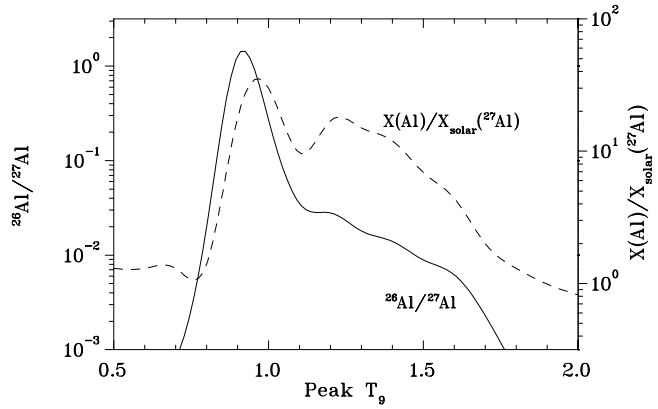

FIG. 4.—Isotopic composition of aluminum shows some of the largest ^{26}Al/^{27}Al ratios ever calculated in any circumstances. These are accompanied by net Al production (*dashed curve*). These facts suggest that the X grain Al can be produced in these circumstances. The ^{22}Na/^{23}Na ratio shows similar effects to those in Al (not shown).

upward without ^{14}N basically bypasses ^{26}Al. In the 16 zone average, the Al abundance is increased by an average factor of 4.

The results for nitrogen are equally significant. Figure 5 shows the ratio of overproductions of its two isotopes in zones differing in $T_{9\,\max}$. This ratio would be equal to 1 for production in solar proportions. The huge overproduction of ^{15}N below $T_9 = 1$ is very evident. This was discovered by Howard et al. (1971) (see their Table 3), who also argued that the explosive He provided the natural source for ^{15}N. However, this idea was abandoned when it was discovered that massive star models do not easily shock their He shells to sufficiently high temperatures and also, and perhaps even more importantly, because in the He-burning shells of these models, the ^{14}N is converted to ^{18}O too soon (prior to supernova shock), thereby rendering the material neutron-rich and causing the flow to bypass these interesting proton-rich nuclei. The He cap atop a Type Ia supernova may revive this idea. But most significant for the puzzling X-type SiC grains, the He cap affords a source of ^{15}N-rich nitrogen that may be related to the ubiquitous excess of that nucleus in those grains. Figure 5 shows the abundance X(N) of N in the zones after ^{15}O decay.

The mean of the 16 zones between $T_9 = 0.5$ and 2.0 yields $Y(\mathrm{N}) = 2 \times 10^{-6}$, which is not small in comparison with solar $Y(\mathrm{N}) = 8 \times 10^{-5}$ and suggests the possibility of significant N substitution in the SiC. This N is overwhelmingly from zones heated to less than $T_9 = 0.8$; therefore, the mass of N revolves about the question of the amount of mass that is not strongly heated. The silicon nitride grains reported by Nittler et al. (1995) were shown to possess isotopic properties relating them to the X-type SiC particles. The large graphite SUNOCONs bearing radioactive (10^5 yr) ^{41}Ca are also characterized by these puzzling excesses of ^{15}N. When averaged over all 16 zones, the N isotopic ratio is close to ^{15}N/^{14}N = 0.4. Furthermore, almost all of that ^{15}N is in the form of its radioactive ^{15}O progenitor at freezeout. With its 122 s half-life, almost none of the ^{15}O can decay during the burning and freezeout, which lasts only a second or so. For $T_9 < 0.5$, the N abundance is larger and is primarily the initial ^{14}N. It is therefore difficult to say what the mean ratio ^{14}N/^{15}N should be, since it depends upon how much matter at lower temperatures exists in the He cap atop a Type Ia supernova. As mentioned above, that matter may also provide the ^{13}C with the ^{12}C-rich carbon.

One of the most exciting features of the type X SiC particles is their tendency to have been condensed while containing live ^{44}Ti (Nittler et al. 1996). It manifests itself as large excesses in the measured ^{44}Ca/^{40}Ca ratio brought about by the decay within the SUNOCON of ^{44}Ti. Although this required presence of live ^{44}Ti identifies the SUNOCON nature of the particle, values of ^{44}Ti/^{48}Ti greater than the solar ratio ^{44}Ca/^{48}Ti are not required. The SiC particles condense the element Ti within them better than they do Ca, so that the Ti/Ca ratio has large positive fractionation (Nittler et al. 1996). It has been known for a long time that He caps in Type Ia supernovae are prolific producers of ^{44}Ti (Woosley, Taam, & Weaver 1986). Our survey confirms that fact. Figure 6 displays the overabundance $\mathcal{O}(^{44}\mathrm{Ca})$ in bulk after the decay, normalized to the overabundance of ^{40}Ca. That ratio increases steeply with peak temperature $T_{9\,\max}$ above 1.5. The figure also shows the ratio of A = 44 production (^{44}Ti) to A = 48 production (^{48}Cr, which quickly decays to stable ^{48}Ti, the most abundant Ti isotope). Figure 7 shows three-dimensional contours at higher temperatures and densities of the final ^{44}Ti mass fraction. Its mountain range–like structure shows that large yields of ^{44}Ti (along with other isotopes in the Ti region) persist with deeper initial conditions. The maximum values for density and temperature in the He cap depend upon its mass. That mass and the models for the Type Ia events themselves (Liebert, Arnett, & Benz 1997) remain very uncertain.

Figure 8 shows the overabundance ratios for other Ti isotopes relative to ^{48}Ti. Because of the large abundance of Ti in SiC, these could all be measured. Of particular interest is the large overabundance of ^{49}Ti in many X grains and in four of the five X grains having huge ^{44}Ca excess (Nittler et al. 1996). The likely interpretation of this (Clayton 1981, which was based on Clayton 1975a; Nittler et al. 1996) is the condensation of ^{49}V, the 330 day parent of ^{49}Ti, prior to

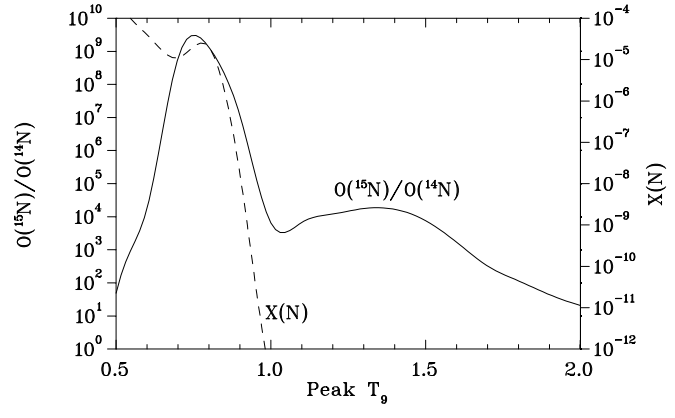

FIG. 5.—Isotopic ratio ^{15}N/^{14}N is shown as a ratio of overproductions with respect to solar composition. The main peak near 0.7–0.9 GK is almost isotopically pure ^{15}N, whose presence in the X grains is a puzzle that might be solved by this scenario for their growth. That ^{15}N is not rare, moreover, is demonstrated by its mass fraction in the matter (*dashed curve*). It is synthesized as ^{15}O by the explosive He burning. Only at the surface is the nitrogen ^{14}N-rich, so that the nitrogen isotopic ratio in the X grains will depend on the mixing within the surface of the He cap prior to SUNOCON growth.

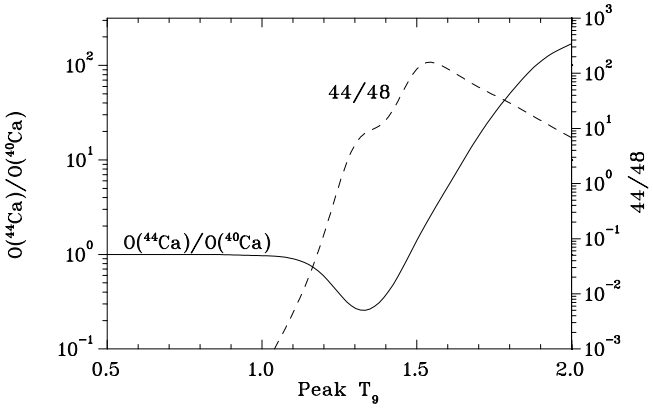

FIG. 6.—Final abundances of ^{44}Ti and of ^{40}Ca are compared as overproduction ratio of ^{44}Ca (to which ^{44}Ti decays during the first century) to ^{40}Ca. This is a bulk ratio and is not equal to that expected in the X grains because they preferentially condense Ti to Ca. Nonetheless, this demonstrates that zones initially above 1.5 GK have sufficient ^{44}Ti for the observed ^{44}Ca richness of the X grains. The dashed curve shows the abundance ratio of the Ti isotopes ^{44}Ti and ^{48}Ti prior to the former's decay. This is presumably the ratio they will condense to in the particles.

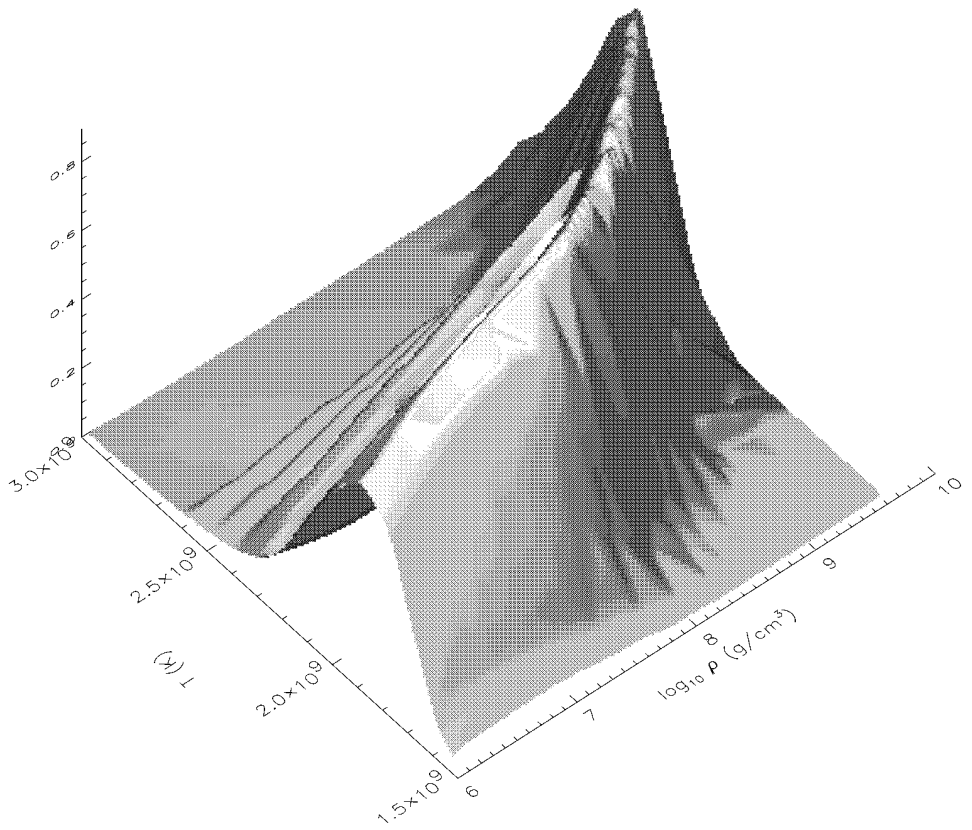

FIG. 7.—Final mass fraction of ^{44}Ti in deeper zones of the He caps of Type Ia supernovae are shown as function of initial temperature and initial density. The stunning ridge of large ^{44}Ti mass reflects the propensity for explosive He burning under such conditions to move the synthesized carbon out to ^{44}Ti before the reactions stall. This feature makes such He caps prolific ^{44}Ti producers. However, these deeper zones will not have the overall chemical composition needed for condensation of X-type SUNOCONs, which are, in our picture, grown primarily from matter heated to peak T less than 1.5 GK.

the ^{49}V decay. This will explain the results if V/Ti is enhanced by chemical fractionation during the condensation of SiC. Unfortunately, this chemical fractionation has not yet been capable of observation owing to the very small abundance of V. These ratios differ greatly from those in Table 2 of Woosley & Weaver (1994) because their yields sum the entire event, whereas ours single out the helium cap. It is exactly this capability of grain condensation to single out a specific chemical environment that gives such a potential for supernova diagnosis.

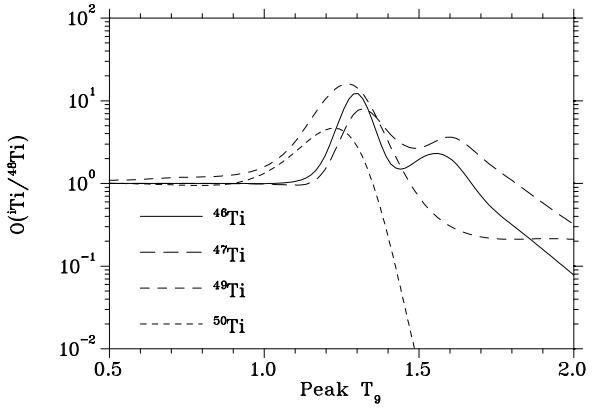

FIG. 8.—Final ratios of Ti isotopes are shown in terms of their calculated overabundances with respect to ^{48}Ti (when normalized to solar ratios). These are of high interest because Ti is a trace element having measurable isotopic composition in the X grains. Of special interest is the ^{49}Ti richness of the X grains; that isotope is arrested at day 330 ^{49}V and therefore condenses as vanadium and only decays within the particle to ^{49}Ti.

Nittler et al. (1996) describe the rather torturous mixing postulates that must be invoked to obtain these particles as Type II SUNOCONs. The problem is that the excess ^{15}N, ^{26}Al, ^{44}Ti, and ^{12}C exist in totally distinct parts of the supernova model and must be chemically "joined" in the year available—without oxidizing the particle! This is difficult in mixing scenarios because oxygen is a principal product in essentially all Type II supernova models. In addition to the hydrodynamic difficulties mentioned above, one wonders why this particular combination of mixing was chosen and why it forms a characteristic class of particles. By contrast, the He cap composition avoids all of those problems. The only mixing may be within the entire He cap itself, each zone of which has isotopic abundances of the desired makeup. None of those zones is oxidizing. The worst that might be said is that the silicon yield Y(Si) is dropping with increasing $T_{9\,\max}$ (Fig. 2) near the $T_9 = 1.5$, where the ^{44}Ti yield steeply rises, and that the ^{15}N-rich matter lies at cooler peak temperatures (Fig. 5). But these are all in proximate layers of the same He cap. This may be a powerful advantage for this model, because a physical reason for the special mixing needed in Type II supernovae has not been found, nor has a plausible mechanism been proposed.

Although the zones are not oxidizing, special mention must be made of the oxygen isotopes. The presolar graphite SUNOCONs bear an ^{18}O excess. The ^{16}O/^{18}O in the SiC X grains has been harder to measure, for there is little

oxygen in SiC; however, in those cases where it has been measured (Nittler et al. 1996), it is clearly ^{18}O-rich. This also presents an obstacle to the scenario of condensation in Type II supernovae, which are prodigious producers of ^{16}O. But in our explosive He survey, the low ^{16}O/^{18}O ratio comes about very naturally. Averaged over zones, $Y(^{16}\mathrm{O}) = 1.5 \times 10^{-4}$, which is about 10 times less than the carbon abundance. But ^{18}F, produced explosively by a single alpha capture on ^{14}N, is quite abundant: $Y(^{18}\mathrm{F}) = 4.4 \times 10^{-5}$; after decay, ^{16}O/^{18}O = 3.4, which is smaller than observed values between 15 and 86 (for the three ^{18}O-rich X grains) but much smaller than the solar ratio of 499. In short, O is abundant, though less so than C, and is ^{18}O-rich, which is quite appropriate for the X grain condensation in a He cap. We must emphasize a subtle difference from the He shell of a Type II presupernova, which is also ^{18}O-rich owing to the ^{14}N(α, γ) reaction. There the ^{18}F has already decayed to ^{18}O, making the matter neutron-rich and spoiling the potential for the correlations we have described. By contrast, in the He cap, for which we have made the critical assumption that it can be emplaced without burning the ^{14}N, the A = 18 isobar is overwhelmingly ^{18}F at the freezeout of the burning and decays thereafter. As such, it is an excellent candidate for early gamma radiation (Leising & Clayton 1987). Its relatively long half-life (1.83 hr) ensures considerable expansion prior to the positron emission, so that significant 511 keV photons may escape to detectors and remain bright for several days. That early 511 keV signal might be detectable from Ia events within the local group, providing a diagnostic of the He cap. After that, the ^{22}Na gamma radiation remains for decades (Clayton 1975b), although it will not be detectable by current gamma-ray technology except in Galactic events of this type.

Table 1 gives the final abundances Y in all 16 zones of differing $T_{9\,\max}$. Because each zone is part of the He cap and because the density gradient could encourage mixing of that cap, some average over the zones may be the most sensible estimate of the likely composition of SUNOCONs that may condense within the ejecta of the He cap. We give three averages in Table 2. One (labeled 1–8) is the average over the zones one through eight, that is, zones reaching peak temperatures from $T_9 = 0.5$ to 1.2. The averaging assumes that each zone contributes an equal mass to the final composition. This first averaging shows the results for the lower temperature zones. By contrast, another averaging gives the results for zones nine through sixteen, that is, peak temperatures from $T_9 = 1.3$ to 2.0. These are the higher temperature zones. The third average gives the results for all sixteen zones. Note that because of the equal weighting of each zone, this third average is the average of the first two averages. The reader may try calculating his or her own averages by using the data in Table 1 and selecting different subsets of the various zones. Such averages may also use unequal weightings of the zones, as the reader sees fit. For now, we simply note that the 1–8 and 9–16 averages usefully distinguish between nuclei primarily made in the low temperature zones (e.g., ^{15}N) and in the high temperature zones (e.g., ^{44}Ti).

In Tables 1 and 2, it is important to note that the abundances are given prior to any radioactive decay. Many abundances are ejected as proton-rich unstable isotopes (with ^{15}O, ^{26}Al, and ^{22}Na being only the more famous cases). The latter two would still exist when the SiC dust

TABLE 2

AVERAGE ABUNDANCES $Y(Z, A)$ IN MOLES PER GRAM

	ZONES AVERAGED OVER		
^AZ	1–8	9–16	1–16
^{1}H.....	7.3E−15	6.4E−15	6.9E−15
^{4}He	2.3E−01	2.0E−01	2.1E−01
^{7}Be.....	3.7E−18	4.0E−26	1.9E−18
^{12}C.....	2.4E−03	2.6E−03	2.5E−03
^{13}C.....	4.9E−11	2.5E−12	2.6E−11
^{14}C.....	1.2E−08	2.7E−25	5.8E−09
^{13}N	2.5E−10	2.5E−12	1.2E−10
^{14}N	3.0E−06	3.7E−17	1.5E−06
^{15}N	5.2E−07	7.3E−16	2.6E−07
^{14}O	1.3E−11	4.3E−19	6.4E−12
^{15}O	6.0E−07	3.7E−17	3.0E−07
^{16}O	2.6E−04	6.7E−06	1.3E−04
^{17}O	2.4E−12	2.3E−17	1.2E−12
^{18}O	1.2E−06	1.3E−14	6.0E−07
^{19}O	2.2E−14	2.5E−26	1.1E−14
^{20}O	9.2E−15	4.7E−16	4.8E−15
^{16}F	1.2E−23	6.3E−16	3.2E−16
^{17}F	3.3E−13	6.1E−20	1.7E−13
^{18}F	8.8E−05	2.9E−13	4.4E−05
^{19}F	2.1E−06	1.6E−14	1.1E−06
^{20}F	3.0E−14	1.9E−15	1.6E−14
^{19}Ne	8.0E−09	2.1E−20	4.0E−09
^{20}Ne	1.5E−04	4.5E−05	9.7E−05
^{21}Ne	9.6E−08	2.6E−09	4.9E−08
^{22}Ne	1.6E−07	1.3E−12	7.9E−08
^{23}Ne	8.9E−16	4.7E−22	4.5E−16
^{24}Ne	1.8E−18	5.0E−24	8.8E−19
^{21}Na	2.3E−12	1.2E−18	1.2E−12
^{22}Na	3.1E−06	1.9E−10	1.6E−06
^{23}Na	6.5E−06	3.2E−10	3.3E−06
^{24}Na	1.8E−09	5.0E−15	9.2E−10
^{25}Na	1.8E−14	1.4E−22	9.1E−15
^{23}Mg.....	2.3E−14	6.6E−23	1.2E−14
^{24}Mg.....	2.5E−04	2.6E−04	2.6E−04
^{25}Mg.....	2.7E−05	1.1E−05	1.9E−05
^{26}Mg.....	3.8E−06	2.5E−09	1.9E−06
^{27}Mg.....	5.1E−11	1.8E−15	2.5E−11
^{28}Mg.....	2.1E−14	1.1E−19	1.1E−14
^{25}Al	2.2E−14	3.7E−24	1.1E−14
^{26}Al	4.7E−06	1.4E−07	2.4E−06
^{27}Al	1.7E−05	1.2E−05	1.4E−05
^{28}Al	2.1E−09	1.3E−10	1.1E−09
^{29}Al	6.9E−12	9.2E−14	3.5E−12
^{27}Si	1.1E−22	3.1E−35	5.4E−23
^{28}Si	6.7E−04	6.4E−04	6.6E−04
^{29}Si	6.3E−06	2.6E−06	4.4E−06
^{30}Si	5.7E−06	7.8E−06	6.7E−06
^{31}Si	5.4E−09	7.2E−10	3.0E−09
^{32}Si	2.0E−12	3.5E−14	1.0E−12
^{29}P	7.5E−21	6.1E−35	3.7E−21
^{30}P	1.2E−07	3.6E−08	7.8E−08
^{31}P	2.3E−06	5.6E−06	3.9E−06
^{32}P	4.9E−10	1.5E−10	3.2E−10
^{33}P	9.5E−11	6.2E−12	5.1E−11
^{31}S	3.4E−22	9.4E−35	1.7E−22
^{32}S	2.6E−04	4.8E−04	3.7E−04
^{33}S	4.3E−07	1.8E−07	3.0E−07
^{34}S	1.4E−06	1.1E−05	6.0E−06
^{35}S	1.1E−09	5.5E−10	8.1E−10
^{36}S	1.9E−09	4.1E−12	9.6E−10
^{37}S	1.6E−13	9.2E−18	8.2E−14
^{38}S	1.4E−16	5.1E−22	7.2E−17
^{35}Cl	8.4E−07	1.6E−05	8.2E−06
^{36}Cl	1.1E−09	1.2E−09	1.1E−09
^{37}Cl	2.0E−08	1.4E−09	1.1E−08
^{38}Cl	2.0E−11	5.2E−14	1.0E−11
^{39}Cl	1.3E−13	7.1E−18	6.7E−14
^{36}Ar.....	2.4E−05	1.2E−03	5.9E−04
^{37}Ar.....	2.8E−08	2.3E−07	1.3E−07
^{38}Ar.....	3.9E−07	4.2E−06	2.3E−06
^{39}Ar.....	6.4E−10	1.3E−11	3.2E−10

TABLE 2—*Continued*

	Zones Averaged Over		
^{A}Z	1–8	9–16	1–16
^{40}Ar	6.0E−10	1.0E−12	3.0E−10
^{41}Ar	1.2E−12	1.2E−16	6.1E−13
^{42}Ar	5.5E−14	1.3E−15	2.8E−14
^{38}K	1.8E−09	1.2E−07	6.1E−08
^{39}K	1.5E−07	2.3E−05	1.1E−05
^{40}K	1.3E−09	1.1E−09	1.2E−09
^{41}K	6.0E−09	1.9E−11	3.0E−09
^{42}K	1.7E−10	5.3E−13	8.3E−11
^{43}K	2.4E−11	5.2E−13	1.2E−11
^{40}Ca	1.5E−06	9.1E−04	4.6E−04
^{41}Ca	1.1E−08	1.9E−07	1.0E−07
^{42}Ca	1.3E−08	8.5E−07	4.3E−07
^{43}Ca	2.5E−09	5.5E−08	2.9E−08
^{44}Ca	3.0E−08	4.0E−09	1.7E−08
^{45}Ca	5.1E−10	6.3E−11	2.9E−10
^{46}Ca	1.2E−10	4.7E−11	8.5E−11
^{47}Ca	2.8E−12	2.1E−12	2.5E−12
^{48}Ca	2.6E−09	1.3E−11	1.3E−09
^{49}Ca	3.3E−12	3.3E−13	1.8E−12
^{50}Ca	4.0E−14	1.7E−11	8.6E−12
^{43}Sc	1.3E−09	1.5E−06	7.7E−07
^{44}Sc	2.2E−10	1.0E−07	5.2E−08
^{45}Sc	2.6E−09	3.3E−08	1.8E−08
^{46}Sc	1.5E−10	4.8E−11	1.0E−10
^{47}Sc	7.3E−11	2.3E−10	1.5E−10
^{48}Sc	1.4E−10	8.7E−11	1.1E−10
^{49}Sc	6.7E−11	2.9E−11	4.8E−11
^{44}Ti	4.4E−10	1.1E−03	5.4E−04
^{45}Ti	4.2E−11	6.8E−07	3.4E−07
^{46}Ti	4.7E−09	1.2E−06	6.3E−07
^{47}Ti	4.0E−09	9.1E−07	4.6E−07
^{48}Ti	4.1E−08	5.1E−09	2.3E−08
^{49}Ti	6.0E−09	1.5E−09	3.7E−09
^{50}Ti	3.9E−09	1.7E−09	2.8E−09
^{51}Ti	2.8E−11	5.0E−11	3.9E−11
^{52}Ti	1.5E−13	5.5E−13	3.5E−13
^{47}V	5.8E−11	3.2E−06	1.6E−06
^{48}V	4.6E−11	8.4E−07	4.2E−07
^{49}V	5.7E−10	3.1E−07	1.6E−07
^{50}V	3.1E−10	1.4E−09	8.5E−10
^{51}V	7.0E−09	2.5E−09	4.7E−09
^{52}V	2.9E−10	2.4E−10	2.6E−10
^{53}V	5.0E−12	1.3E−11	9.0E−12
^{48}Cr	3.1E−12	8.5E−05	4.2E−05
^{49}Cr	1.1E−12	1.1E−06	5.4E−07
^{50}Cr	1.3E−08	2.9E−06	1.5E−06
^{51}Cr	9.9E−10	7.0E−07	3.5E−07
^{52}Cr	2.8E−07	4.7E−08	1.6E−07
^{53}Cr	3.4E−08	4.9E−09	1.9E−08
^{54}Cr	1.4E−08	1.5E−08	1.5E−08
^{55}Cr	1.5E−10	6.1E−10	3.8E−10
^{56}Cr	1.5E−11	1.9E−10	1.0E−10
^{51}Mn	2.4E−11	3.1E−06	1.6E−06
^{52}Mn	1.5E−11	7.9E−07	4.0E−07
^{53}Mn	1.0E−09	7.9E−07	3.9E−07
^{54}Mn	2.2E−10	1.5E−09	8.7E−10
^{55}Mn	2.2E−07	1.7E−08	1.2E−07
^{56}Mn	5.3E−12	9.5E−11	5.0E−11
^{57}Mn	2.5E−10	8.3E−10	5.4E−10
^{50}Fe	4.6E−18	1.9E−10	9.4E−11
^{52}Fe	3.0E−13	1.4E−05	7.2E−06
^{53}Fe	5.7E−14	3.8E−07	1.9E−07
^{54}Fe	1.2E−06	1.3E−06	1.2E−06
^{55}Fe	6.1E−08	1.1E−07	8.7E−08
^{56}Fe	2.0E−05	2.4E−06	1.1E−05
^{57}Fe	1.1E−06	5.9E−07	8.3E−07
^{58}Fe	2.6E−07	1.3E−06	8.0E−07
^{59}Fe	1.9E−08	3.3E−07	1.7E−07
^{60}Fe	2.5E−09	2.4E−07	1.2E−07
^{55}Co	6.8E−10	5.3E−07	2.6E−07
^{56}Co	1.1E−09	6.8E−08	3.5E−08
^{57}Co	2.9E−08	1.3E−06	6.9E−07

TABLE 2—*Continued*

	Zones Averaged Over		
^{A}Z	1–8	9–16	1–16
^{58}Co	5.4E−09	5.9E−08	3.2E−08
^{59}Co	6.0E−08	1.3E−06	6.9E−07
^{60}Co	5.4E−09	3.1E−07	1.6E−07
^{61}Co	1.8E−09	3.2E−08	1.7E−08
^{54}Ni	2.5E−21	2.2E−13	1.1E−13
^{56}Ni	1.6E−12	4.7E−07	2.3E−07
^{57}Ni	7.9E−13	1.2E−07	6.0E−08
^{58}Ni	7.7E−07	1.8E−06	1.3E−06
^{59}Ni	3.8E−08	7.3E−07	3.8E−07
^{60}Ni	3.3E−07	3.0E−06	1.6E−06
^{61}Ni	3.2E−08	1.0E−06	5.4E−07
^{62}Ni	5.3E−08	1.1E−06	5.5E−07
^{63}Ni	5.9E−09	1.9E−08	1.2E−08

condenses (assuming that it does so), but the ^{15}O will have decayed before.

4. THE He CAP AND ITS IGNITION

First, it is important to emphasize that the nature of the progenitors of Type Ia supernovae and their evolution to explosion are far less well understood than that of Type II supernovae (see Liebert et al. 1997, for example, and Arnett 1996, pp. 451–458). This means that we have less certainty as to whether the conditions we require are satisfied in nature.

Take the most popular model, which supposes that the Type Ia supernova is the result of degenerate ignition of ^{12}C in a white dwarf near the Chandrasekhar limiting mass. An outer ^{4}He layer can extend down to a density of 1.15×10^{6} g cc^{-1} (beyond which electron capture will occur on ^{14}N), which gives a thermal runaway (Hashimoto et al. 1986). Thus, the ratio of He shell density to central density must be less than about 10^{-3}, which implies a mass in the He layer of 0.01 $M_{\odot}$ or less. If this is the correct site, the small mass of such He caps limits the Galactic ejection rate for these caps to $10^{-2} M_{\odot}$ per century, or about 10^{-5} $M_{\odot}$ per century of SiC grains, given efficient condensation.

A larger fraction of the white dwarf can be in the He layer if the central density is lower, that is if the total mass is less than the Chandrasekhar limit. Here, however, the ignition is supposed to be from a point detonation in the He layer. At higher densities of He (near the electron capture limit), the detonation will burn much of the He into Ni (Woosley & Weaver 1994), even in the correct two-dimensional geometry (Livne & Arnett 1995). Nevertheless, the lower density parts of the He layer do undergo burning somewhat reminiscent of that described here. The total ejection rate of SiC grains can be only moderately greater than before, however, if the frequency of such events is restricted by the requirement that ^{44}Ca not be overproduced. Dynamic one-dimensional studies show that ^{44}Ca is overproduced relative to ^{56}Fe for low-mass (0.6–0.7 $M_{\odot}$) white dwarfs, but not for more massive ones (Woosley & Weaver 1994; see their Table 3). Those He caps have masses near 0.2 $M_{\odot}$. A qualitatively similar result is obtained in two dimensions (Livne & Arnett 1995), with the detonation from a point (rather than the unlikely synchronized detonation of a spherical shell as is imposed in one dimension).

In both cases, the He layer is one of the highest velocity parts of the ejecta, barring instabilities. Without a clear picture of the event, it is difficult to be more specific. We

note that instabilities may occur between the CO core and He cap during shock and ignition. These need not mix the compositions during the burning timescale, but they might importantly mix the velocity profile of the total ejecta. They might produce fast CO ejecta penetrating through some residual, slower, He. The importance of "slow He" is that the SiC particles have a much better chance of growing in slow He than in spherical models, where all of the He is very fast. For homologous expansion after some early reference time t_0, the particle densities governing the growth of SiC decline as $\rho(t) = \rho_0(t_0/t)^3$, where ρ_0 is the density at t_0 when the grain temperatures have fallen to near 2500 K. The initial density at 2500 K will be greater within slow He imbedded deeper within the velocity profile, if such imbedding occurs. It is a long extrapolation from the burning instabilities (perhaps the first few seconds) to the long-time (months) structure of the clumpy ejecta. It will also be instructive to calculate chemical aspects of the growth of both graphite and SiC along lines introduced by Bernatowicz et al. (1996).

The growth of SiC takes us thereby into issues beyond the intended scope of this paper, whose goal centers on the similarity of compositions. The grain growth must, furthermore, take into account the non-LTE nature of the chemical condensation. The grains, being somewhat free to radiate, will have smaller temperatures than the kinetic temperature of the particles, so that SiC might be stable unexpectedly early. The radiation field is also very non-LTE, because it has an intense high-energy tail from the Compton scattering of the gamma rays from ^{56}Co (primarily). These considerations await future work.

This research was supported by grants from NASA Planetary Materials and Geochemistry Program to D. D. C. and to B. S. M, by NASA grant NAGW-2450 and NSF grant ASTRO 9015976 (D. A. and J. K.), and by DOE contract W-7405-ENG-48 to Lawrence Livermore National Laboratory (J. K.).

REFERENCES

Amari, S., Hoppe, P., Zinner, E., & Lewis, R. S. 1992, ApJ, 394, L43
Amari, S., Zinner, E., & Lewis, R. S. 1996, ApJ, 470, L101
Arnett, D. 1994, ApJ, 427, 932
———. 1996, Supernovae and Nucleosynthesis (Princeton: Princeton Univ. Press)
———. 1997, Thermonuclear Supernovae, ed. P. Ruiz-Lapuente, R. Canal, & J. Isern (Dordrecht: Kluwer), 405
Bazan, G., & Arnett, D. 1994, ApJ, 433, L41
———. 1997, ApJ, submitted
Bernatowicz, T. J., Cowsik, R., Gibbons, P. C., Lodders, K., Fegley, B., Amari, S., & Lewis, R. S. 1996, ApJ, 472, 760
Clayton, D. D. 1975a, Nature, 257, 36
———. 1975b, ApJ, 198, 151
———. 1977, Earth Planet. Sci. Lett., 36, 381
———. 1981, Proc. Lunar Planet. Sci., 12B, 1781
Clayton, D. D., & Wickramasinghe, N. C. 1976, Ap&SS, 42, 463
Hashimoto, M., Nomoto, K., Arai, K., & Kiminishi, K. 1986, ApJ, 307, 687
Hoppe, P., Amari, S., Zinner, E., Ireland, T., & Lewis, R. S. 1994, ApJ, 430, 870
Hoppe, P., Amari, S., Zinner, E., & Lewis, R. S. 1995, Geochim. Cosmochim. Acta, 59, 4029
Hoppe, P., Geiss, J., Buehler, F., Neuenschwander, J., Amari, S., & Lewis, R. S. 1993, Geochim. Cosmochim. Acta, 57, 4059
Hoppe, P., Strebel, R., Eberhardt, P., Amari, S., & Lewis, R. S. 1996a, Geochim. Cosmochim. Acta, 60, 883
———. 1996b, Science, 272, 1314
Howard, W.M., Arnett W. D., & Clayton, D. D. 1971, ApJ, 165, 495
Kane, J., Arnett, D., Remington, B. A., Glendinning, S. G., Castor, J., Rubenchik, A., & Fryxell, B. A. 1996, ApJ, submitted
Kutschera, W., & Paul, M. 1990, Ann. Rev. Nucl. Part. Sci., 40, 411
Leising, M. D., & Clayton , D. D. 1987, ApJ, 323, 159
Liebert, J., Arnett, D., & Benz, W. 1997, Advanced Stellar Evolution, ed. R. Rood (Cambridge: Cambridge Univ. Press), in press
Livne, E., & Arnett, D. 1995, ApJ, 452, 62
Meyer, B. S., Krishnan, T. D., & Clayton, D. D. 1996, ApJ, 462, 825
Meyer, B. S., Weaver, T. A., & Woosley, S. E. 1995, Meteoritics, 30, 325
Nittler, L. R., Amari, S., Zinner, E., Woosley, S. E., & Lewis, R. S. 1996, ApJ, 462, L31
Nittler, L.R., et al. 1995, ApJ, 453, L25
The, L.-S., et al. 1995, ApJ, 444, 244
Timmes, F. X., Woosley, S. E., Hartmann, D. H., Hoffman, R. D., Weaver, T. A., & Matteucci, F. 1995, ApJ, 449, 204
Woosley, S. E., Taam, R. E., & Weaver, T. A. 1986, ApJ, 301, 601
Woosley, S. E., & Weaver, T. A. 1994, ApJ, 423, 371